DESIGN AND CHARACTERIZATION OF A QUASI-OPTICAL SIS RECEIVER FOR THE 1 THZ BAND

M. Bin, M. C. Gaidis, D. Miller, J. Zmuidzinas, and T. G. Phillips

George W. Downs Laboratory of Physics, 320-47, California Institute of Technology, Pasadena, CA 91125.

H. G. LeDuc

Center for Space Microelectronics Technology, Jet Propulsion Laboratory, 302-231, Pasadena, CA 91101.

Abstract–We report on the design and characterization of broadband quasi-optical SIS receirvers for the 1 THz frequency band. The mixer design utilizes a twin-slot antenna, an antireflection-coated silicon hyperhemispherical lens, Nb/Al-oxide/Nb tunnel junctions, and an aluminum normal-metal tuning circuit in a two-junction configuration. The frequency response of the device was measured using a Fourier transform spectrometer and agrees reasonably well with the theoretical prediction. Heterodyne tests were carried out from 822-1042 GHz and low receiver noise temperatures of about 770 K were obtained after correcting the losses from the LO/signal beamsplitter.

I. Introduction

The best quasi-optical and waveguide Nb/Al-oxide/Nb SIS mixers with Nb tuning structures have achieved noise temperatures within a factor of 10 of the quantum limit ($T_{ql} = h\nu/k_B$ for the single-sideband noise temperature) at frequencies below the Nb gap ($\nu < 700$ GHz).[1] Recently good results were also obtained in the 800 GHz band with all-Nb mixers.[2,3,4] Theoretically, heterodyne mixing in SIS devices is useful up to twice the gap frequency.[5,6,7] However, the RF loss of superconductors increases significantly above the gap frequency because the RF photons have sufficient energy to break Cooper pairs. This causes a larger fraction of the incoming radiation to be dissipated in the superconducting electrodes and tuning structures. To reduce this RF loss, tuning circuits made of a high conductivity normal metal such as aluminum have been fabricated [8,9] and encouraging receiver performace has been obtained.

This paper will give a more detailed analysis on our previously reported 1 THz quasi-optical SIS mixer with normal-metal Al tuning circuits.[8] The Nb/Al mixer design incorporates a twin-slot antenna, a two-junction configuration, and an antireflection-coated silicon hyperhemispherical lens. A thorough description of the mixer optics, layout, and equivalent circuit can be found in a paper by Gaidis et al.[10] Surface impedance calculation of superconducting and normal-metal films will be presented in section II. The mixer design and modeling will be discussed in section III. Section IV will describe the mixer performance in direct detection mode and heterodyne mode. Finally, we discuss the contributions of various components to the receiver noise temperature in section V.

II. Surface Impedance and Microstrip Lines

Understanding the characteristics of microstrip transmission lines at high frequencies is critical for the design of SIS mixers. A microstrip line can be modeled as a ladder of series impedance Z and shunt admittance Y, with series resistance R and inductance L, shunt conductance G and capacitance C per unit length of the line. R describes the conductor loss, which is for most cases

much larger than the loss in dielectric described by G. The characteristic impedance of the line is given by

$$Z_0 = \sqrt{\frac{Z}{Y}} = \sqrt{\frac{(R + j\omega L)}{(G + j\omega C)}} \tag{1}$$

The propagation constant $\gamma = \alpha + j\beta$ is determined by

$$\gamma = \sqrt{ZY} = \sqrt{(R + j\omega L)(G + j\omega C)} \tag{2}$$

with α the attenuation constant and β the phase constant.

Non-ideal conductors have a surface impedance Z_s which affects the characteristic of microstrip lines. For a thin conductor film of thickness d the surface impedance is defined for a sinusoidal electric field $E_x(z,\omega)$ and current density $J_z(z,\omega)$ by [11]

$$Z_s(\omega) = \frac{E_x(0,\omega)}{\int_0^d dz J_x(z,\omega)} \tag{3}$$

The real part of Z_s, called the surface resistance, accounts for microstrip losses and the imaginary part, the surface reactance, contributes to the microstrip line inductance.

A. Normal Conductors

When the eletric field penetration depth is long compared to the electron mean free path, the local equation can be assumed for the relation between current **J** and field **E**. Solving Maxwell equations in the local theory we obtain normal skin effect surface impedance:

$$Z_s = (i\omega\mu_0/\sigma)^{1/2} \coth[(i\omega\mu_0\sigma)^{1/2} d] \tag{4}$$

where σ is the conductivity and d is the thickness of the conductor.

When the penetration depth is comparable with the electron mean free path l, which is often true at high frequencies and cryogenic temperatures, a non-local form must be assumed for **J** and **E**. Following the arguments of Pippard,[12] the electric field can be obtained by solving an integro-differential equation:

$$\frac{d^2 E_x}{dz^2} = i\alpha l^{-3} \int_0^d dz' E_x(z') K((z' - z)/l) \tag{5}$$

$$K(u) = \int_1^\infty dr[1/r - 1/r^3] e^{-|u|r} \tag{6}$$

where $\alpha = 3l^2/2\delta_c^2$. Here δ_c is the classical penetration depth:

$$\delta_c = \sqrt{\frac{2}{\mu_0\omega\sigma}} \tag{7}$$

The skin effect under such conditions is called anomalous. A method to calculate Z_s for the anomalous skin effect using the equations above is given by Kautz.[11] In the limits of infinite conductor thickness ($d \to \infty$) and the extreme anomalous case ($\alpha \gg 1$), a simple equation is obtained by Reuter and Sondheimer

$$Z_s = \frac{1}{3^{1/2}\pi^{1/3}}(1 + \sqrt{3}i)\frac{\alpha^{2/3}}{\sigma l} \tag{8}$$

For Al the conductivity is a real constant. For instance, the resistivity ρ of Al at room temperature is 2.45 $\mu\Omega$-cm, which corresponds to an electron mean free path l of 16 nm.[13] At lower

temperatures, the resistivity can be much lower than this value. Since the product ρl is independent of temperature,[13] and l is often limited by the conductor thickness in the case of a thin film, the amount of decrease in ρ for a thin film can be less than that for a bulk conductor. The resistivity ratio $\Re = \rho_{300K}/\rho_{4k}$ for Al film of 200 nm thick is limited to 200 nm/16 nm $\approx$ 12. In practice we have measured a resistivity ratio of $\Re \approx 5$ at 4.2 K for 200 nm thick Al film, which is equivalent to $\rho_{4K} \approx 0.5$ $\mu\Omega$-cm. The penetration depth at submillimeter frequencies and liquid helium temperature is a few tens of nanometers. Thus, the mean free path is larger than the penetration depth and is comparable to the film thickness, and we must apply the anomalous skin effect theory to calculate the surface impedance. An anomalous surface impedance result obtained by solving Eq. (5) and (6) is shown in Fig. 1 for an Al film of thickness 200 nm. For comparison, the results obtained with normal skin effect formula Eq. (4) and the extreme anomalous formula Eq. (8) are also presented in Fig. 1. It is worth noting that while the normal skin effect result is close to the anomalous one in the submillimeter region, the extreme anomalous result underestimates the surface resistance by almost 40%.

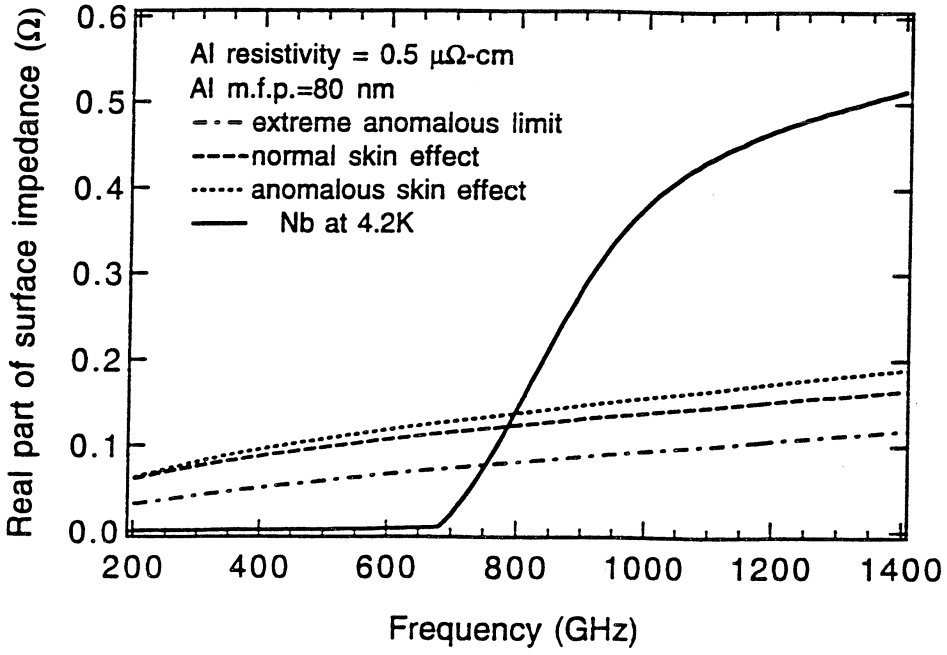

Fig. 1. The calculated surface impedance of normal-metal Al and superconducting Nb films at 4.2 K. The film thickness is 200 nm. The Al resistivity is 0.5 $\mu\Omega$-cm, or 1/5 the room teperature value. The normal state conductivity of Nb at transition temperature is 5 $\mu\Omega-$cm.

B. Superconductors

For superconductors the surface impedance should be computed by solving the non-local Mattis-Bardeen theory [14] for a thin film as done by Pöpel. [15] This procedure can be simplified somewhat if the films are thick enough to use a bulk limit approximation. Actually Pöpel found that if the thickness is more than three times of the superconducting penetration depth, then the bulk limit solution is a very good approximation to the exact solution. We simplified further by using Mattis-Bardeen theory in the extreme anomalous limit and obtained the complex conductivity for

the superconductor. The surface impedance is then calculated by placing this complex conductivity into the normal skin effect formula Eq. (8). We found good agreement between our approximate local-limit calculation and the complete non-local Mattis-Bardeen solutions for very thick films. [16]

C. Microstrip Lines

The characteristic impedance, phase velocity and loss of the microstrip lines are calculated in the manner described by Zmuidzinas.[17] First the behavior of a microstrip line made from a perfect conductor ($\sigma = \infty$) is calculated using the design equations given by Hammerstad and Jensen.[18] This gives the series impedance Z and the shunt admittance Y per unit length of the line. The effect of replacing the perfect conductor by the real conductor is approximated by introducing an extra contribution to the series impedance of the line: $Z' = Z + gZ_s$, where Z_s is the surface impedance of the line and g is a geometrical factor.

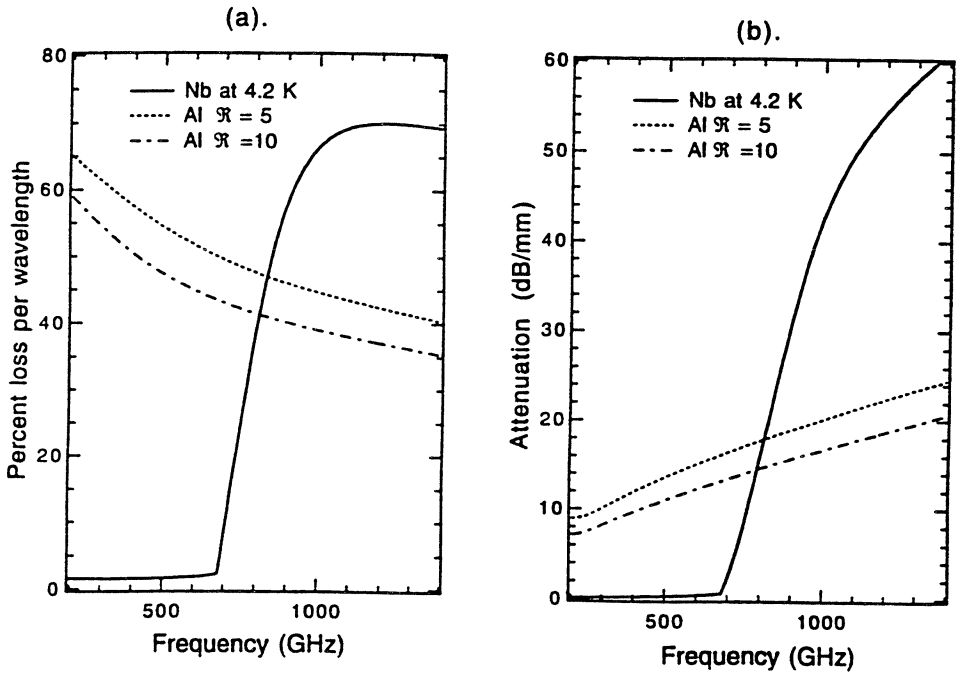

Fig. 2. The calculated frequency dependence of (a) the power loss per wavelength and (b) the attenuation per unit length for 5 μm wide microstrip lines. The insulation layer is 400 nm SiO and the metal thickness is 200 nm. Calculations are made for temperature at 4.2 K. Two resistivity ratios ($\Re = \rho(300\text{ K})/\rho(4.2\text{ K})$) 5 and 10 are used for the Al film in the calculations; the room temperature resistivity is assumed to be 2.45 $\mu\Omega$ cm.

While the surface impedance introduces changes in characteristic impedance and phase velocity to the microstrip line, it is the loss caused by the surface impedance that we are most concerned with. As an example, we have calculated the percent power loss per wavelength and the attenuation per unit length for a microstrip line. The microstrip line has a typical dimension used in the SIS tuning circuit: 5 μm width, 400 nm SiO insulation layer thickness, and the 200 nm metal thickness. The results are shown in Fig. 2 for superconducting Nb and normal-metal Al microstrip lines. Note that

the loss in the Nb line is negligible below gap frequency, but increases dramatically above 700 GHz and eventually has the same trend as a normal-metal line. Our calculation shows that the Al line is comparable in loss performance with Nb line at 830 GHz, but becomes a better choice at higher frequencies.

III. Mixer Design and Fabrication

We adopt the twin-slot double-junction mixer design with an anti-symmetric feed.[19] This design has the advantage that no dc-blocking capacitance is needed in the tuning circuit. Fig. 3 shows how this is realized. The RF circuit design is symmetric about the center. The center microstrip connecting the two junctions serves as the tuning inductor L. The two transmission lines connecting the junctions to the slots are impedance transformers. The two radial stubs are the feed points of the twin-slot antenna and couple the radiation into the transmission lines. Since the radial stubs sit at the opposite side of the slots, the two feeding signals are 180 degrees out of phase. This antisymmetric feed produces a virtual ground at the center of the tuning inductance L, so each junction is effectively shunted by an inductance of $L/2$.

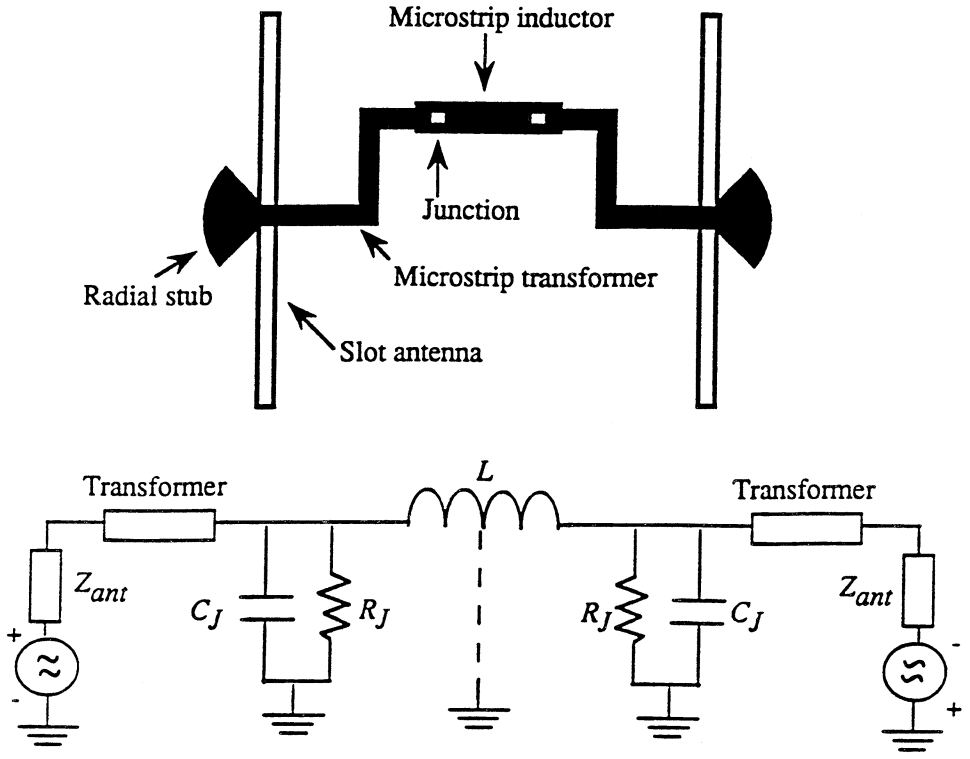

Fig. 3. A typical mixer layout and the equivalent circuit. The layout is not to scale.

The microstrip lines are made from normal-metal Al of $\approx$ 200 nm thick. The insulation layer is made from SiO with a relative dielectric constant of 5.6. There is a 5 μm wide, 2.5 μm long microstrip as a spacer connecting the junction and the impedance transformer. The SiO thickness for the center inductor and the spacer are 200 nm. The SiO thickness for the impedance transformer

is increased to 400 nm to better optimize the impedance match to the slot antenna. The design is done by optimizing the calculated RF coupling efficiency in the 1000-1100 GHz bandwidth with the widths and lengths of the inductor and transformer sections as free parameters.

The RF coupling efficiency is defined as the ratio of absorbed power at the junction to the available power at the source. The source impedance is that of the twin-slot antenna, which is calculated by the method of moments.[17] We assume that the junction has a normal-state resistance-area product $R_N A = 20\ \Omega\mu\text{-m}^2$ (corresponding to $J_c \approx 10\ \text{kA/cm}^2$). The circuit is optimized for a junction of area $1.3 \times 1.3\ \mu\text{m}^2$. The junction RF impedance is calculated from Tucker's theory [20] in the small signal approximation and includes both RF resistance and quantum reactance. The junction specific capacitance was not known accurately beforehand, so we optimized our circuit for two values: 65 and 85 $\text{fF}/\mu\text{m}^2$. For each optimized tuning circuit, we also implement mixers with juncton areas of $1.1 \times 1.1\ \mu\text{m}^2$ and $1.5 \times 1.5\ \mu\text{m}^2$. Fig. 4 shows the equivalent circuit with the corresponding Smith chart plot of the RF impedances. The inductance section brings the capacitive part of the SIS junction into a real impedance at the center of the frequency. The transformer section then transforms the impedance up to match the antenna impedance.

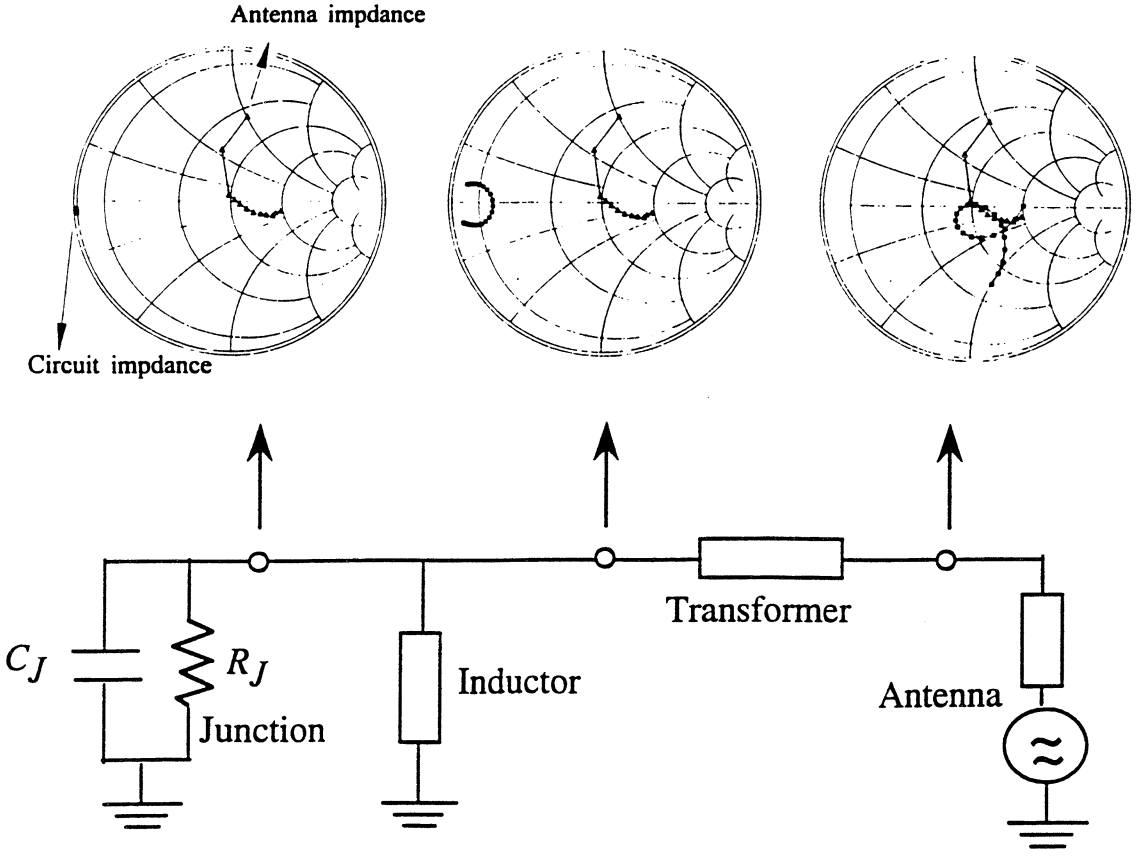

Fig. 4. The equivalent anti-symmetric tuning circuit with Smith charts showing the impedance at each position of the circuit from 860 GHz to 1260 GHz. The Smith chart is normalized to 30 Ω. The impedances shown in the Smith charts are towards the junction with the circuit towards the antenna disconnected. The complex antenna impedance is also shown in the Smith charts for comparison.

During our design we assumed a resistivity ratio $\Re = 10$ for the Al film. In practice the resitivity

ratio is measured to be 5. The RF coupling responses calculated using $\Re = 10$ or 5 are quite similar in shape with the one for $\Re = 5$ reduced in amplitude by about 20%. The final response calculated for the real mixer is presented in Fig. 5.

The Nb/Al devices were fabricated on 50 mm diameter, 0.25 mm thickness high-resistivity silicon wafers using a modified Nb/Al-oxide/Nb junction process. First, a 200 nm aluminum ground plane was deposited, followed *in-situ* by the Nb/Al-oxide/Nb trilayer. The ground plane and slot antennas are patterned in this step using a liftoff technique. The junctions are defined with optical lithography and are formed by reactive ion etching (RIE) of the Nb/Al-oxide/Nb trilayer. All of the unprotected Nb must be removed so that the Al ground plane is exposed for the microstrip lines. The junctions are isolated with a 200 nm SiO film patterned by self-aligned liftoff, and a second 200 nm SiO film is added to produce a total SiO thickness of 400 nm for the impedance transformer. The 200 nm Al wiring layer is deposited and patterned as the last step.

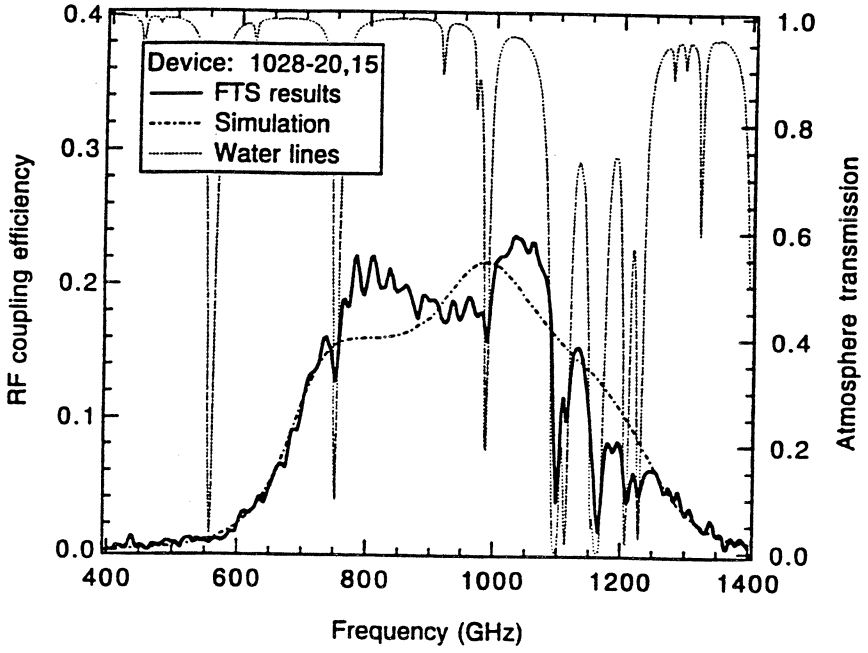

Fig. 5. Direct detection response measured with the FTS. The heavy dashed line is the calculated RF coupling efficiency. The atmospheric transmission is calculated assuming a relative humidity of 13% and a path of 3 meters.

IV. Receiver Performance

A. Receiver Optics

The receiver optics consists of a Mylar LO injection beamsplitter, a dewar vacuum window, a 77 K IR filter, a polyethylene lens at 4 K, and an antireflection (AR) coated silicon hyperhemispherical lens. We use three different thickness Mylar beamsplitters, 10 μm, 25 μm and 50 μm, depending on the available LO power. The reflectivity of the three beamsplitters at 1000 GHz are 7.5%, 30% and 43% respectively. For the vacuum window we have used a 25 μm Mylar, which has a transmission of 82% at 1000 GHz, and an AR-coated 2.2 mm thick quartz plate. This quartz

window is AR-coated for center frequency at 850 GHz, with a calculated transmission of 94%. The transmission oscillates with a period of $\approx$ 30 GHz. The lowest value in the frequency range of interest is about 87%. For the 77 K IR filter, we tried a clear 2.2 mm quartz plate and an AR-coated 2.2 mm quartz plate. The clear quartz filter has resonating transmissions from 60% to 100% depending on the frequency. The AR-coated quartz filter is centered at 814 GHz with peak transmission of 97%. The AR coating on the hyperhemisphere was optimized for 850 GHz and has 85% transmission at 1000 GHz.

B. Direct Detection Response

The device we report here has a nominal area of 1.3×1.3 μm^2 and was optimized assuming a specific capacitance of 85 fF/μm^2. The normal state resistance of the junction is 13 Ω. The response of the device as a function of frequency was measured with a built-in-house Fourier-transform spectrometer (FTS) using the SIS as a direct detector. This gives a direct measure of the RF coupling efficiency.[21,22] Fig. 5 shows an FTS result along with the response predicted by the circuit simulation. Since the optical coupling efficiency is not well known, we cannot yet obtain an absolute response. Nontheless, the shape of the response is a good diagnostic of the tuning circuit. To compare the measured response with the theoretical predictions, we scaled the vertical axis of the experimental curve to match the simulation one. Note that the simulation predicts the shape of the response quite well as a whole except some fine structures. The experimental data above 1100 GHz is affected by the strong absorption lines caused by the residual water vapor that is present in our nitrogen-flushed FTS system. Additional non-idealities are the resonant peaks approximately 30 GHz apart caused by Fabry-Perot resonances in the AR-coated quartz IR filter. Since the lossy tuning circuit has a low Q, the device has an extremely wide bandwidth of about 450 GHz.

C. Heterodyne Tests

The receiver noise temperature was measured using the standard Y-factor method with a hot load at 295 K and a cold load at 80 K. In these tests, the total intermediate frequency (IF) power was measured in a 1 GHz bandwidth centered at 1.5 GHz. The low temperature IF amplifier is a Lange-coupler-balanced two-stage GaAs HEMT unit built by Jacob Kooi.

1042 GHz

Local oscillator power at 1042 GHz was generated using a difluoromethane (CH_2F_2) far-infrared laser, pumped by a $\lambda = 10$ μm CO_2 laser. Since this LO was very powerful, we used 10 μm thick mylar beamsplitter. The pressure window was 25 μm Mylar and the IR filter was the 2.2 mm clear quartz plate. The best uncorrected DSB receiver noise temperatures were 1170 K at 4.2 K, and 840 K when the device was cooled to $\approx$2 K.

982 GHz

LO power at 982 GHz was obtained using a fixed-tuned solid-state Gunn/multiplier LO provided by Peter Zimmerman. For these tests, we used the AR-coated 2.2 mm quartz pressure window and the AR-coated 2.2 mm quartz IR filter. Although the LO was estimated to produce $\approx$ 60 μW at 982 GHz, we could not obtain optimum pumping with 25 μm Mylar beamsplitter. When a 50 μm Mylar beamsplitter was used, we got close to optimum pumping but the receiver noise temperature increased (as expected). The uncorrected DSB receiver noise temperature is 1466 K with 25 μm beamsplitter at 4.2 K bath temperature and 1307 K at 2 K bath temperature.

822 Ghz and 852 GHz

We also tested the device at 822 GHz and 852 GHz using a tunable InP Gunn oscillator followed

by a cascaded (×2×3) GaAs Schottky varactor multiplier from Peter Zimmerman. The same pressure window and 77 K IR filter as for the 982 GHz test were used. We obtained just enough LO power with the 25 μm beamsplitter. The uncorrected DSB receiver noise temperature is 1420 K at 4.2 K bath temperature and 1207 K when the device was cooled to 2 K.

TABLE I. Receiver noise temperature

f_{LO} (GHz)	vacuum window & IR filter	uncorrected DSB receiver noise $T_{receiver}$				corrected $T_{receiver}$	
		2 mil BS @4.2 K	1 mil BS @4.2 K	2 mil BS @2 K	1 mil BS @2 K	@4.2 K	@2 K
822	qtz.; AR qtz.	1727 K	1334 K	1549 K	1207 K	846 K	756 K
852	qtz.; AR qtz.	1727 K	1420 K	1561 K	1207 K	857 K	757 K
982	qtz.; AR qtz.	–	1466 K	1587 K	1307 K	938 K	777 K
1042	Mylar; cl. qtz	1170 K, 0.45 mil BS		840 K, 0.45 mil BS		1050 K	752 K

Table I summarizes the receiver noise temperatures for the device under different testing conditions. DSB receiver noise temperatures corrected for the beamsplitter are also listed. At about 2 K this device gives low-noise performance in a wide band 822-1042 GHz with a corrected DSB noise of $\approx$ 770 K.

Discussions and Conclusions

Beamsplitter

It is obvious from Table I that thicker Mylar beamsplitters increase the receiver noise temperature. A significant improvement in the uncorrected noise temperatures could be achieved if we had enough LO power and used the 10 μm beamsplitter instead of the 25 μm beamsplitter, or if we used a LO injection deplexer. From experience we find that the optimum pumping is obtained when $\alpha = eV_{LO}/h\nu = 0.6$. The LO power absorbed by the junction can be estimated as [20]

$$P_{LO} \approx V_{LO}^2/2R_N \approx \frac{1}{2}\frac{(0.6h\nu/e)^2}{R_N} \tag{10}$$

For a single junction of $R_N \approx 13\ \Omega$ and at 1000 GHz, $P_{LO} \approx 236$ nW. Since there is a lack of LO power at high frequencies, making smaller junctions would help. Existing submicron junction technology could reduce the LO power needed for optimum pumping by a factor of six.

Cooling to 2 K

When the mixer was cooled to 2 K, the noise temperature dropped from 1170 K to 840 K at 1042 GHz. The 40% improvement in the receiver noise temperature at the lower temperature can be largely explained by the reduction in the subgap leakage current ($\approx$ 10 μA) and the increase in the gap voltage ($\approx$ 0.2 mV). Tucker theory[20] calculations indicate that these effects result in a 20% drop in the mixer noise temperature and a 35% reduction in the conversion loss. Therefore, a 25-30% reduction in the receiver noise temperature can be expected from these effects. The remaining 10-15% improvement that is unaccounted for may be due to a reduction in the microstrip loss at the lower temperature.

IF Chain Calibration

We have used the shot-noise technique[23,24] to estimate the IF noise temperature and the receiver conversion loss at 1042 GHz and 4.2 K, and obtained reasonably good agreement between experimental measurement and theoretical prediction.[8] Here we analyze the experimental data taken at 852 GHz and 4.2 K with a 50 μm Mylar beamsplitter. The same shot-noise technique gave $T_{\rm IF} = 6$ K and $L_{\rm conv} = L_{\rm RF}L_{\rm mixer} = 18$ dB (DSB), after taking into account the IF port mismatch, gave This value of $T_{\rm IF}$ agrees with independent measurements of the HEMT IF amplifier noise temperature. The total RF signal losses in the receiver, including the optics and the Al microstrip circuit, are estimated to be $L_{\rm RF} \approx 9.0$ dB (see Table II).

TABLE II. Estimated contributions to receiver conversion loss and noise temperature

Components	Estimated transmission t	Loss in dB	Temperature (K)		Noise Temperature (K)
			$T_{\rm phys}$	$T_{\rm equiv}$	$T_{\rm n} = (1-t)T_{\rm equiv}/t$
50 μm Mylar beamsplitter	0.57	2.44	295	275	208
Quartz dewar window	0.94	0.27	295	275	18
IR quartz filter	0.96	0.18	77	58	2.4
Polyethelene lens	0.95	0.22	4.2	0.003	0.0
Silican lens and antenna	0.85	0.7	4.2	0.003	0.0
Al microstrip circuit	0.30	5.3	4.2	0.003	0.0
Total optical and RF loss $L_{\rm RF} = 9.0$ dB			Total contrib. noise $T_{\rm RF} = 244$ K		
Estimated mixer conversion loss $L_{\rm mixer} = 9.1$ dB			Estimated $T_{\rm mixer} = 139$ K		
Theoretical mixer conversion loss $L_{\rm mixer} = 7.9$ dB			Theoretical $T_{\rm mixer} = 126$ K		

We also estimated the noise contributions from the optics components by the simple argument that for each lossy component with transmission t, the noise temperature is

$$T_n = (1-t)T_{\rm equiv}/t \tag{10}$$

Here $T_{\rm equiv}$ is the equivalent temperature of a blackbody of physical temperature $T_{\rm phys}$ which gives the same amount of radiation in the Rayleigh-Jeans limit as that given by the Planck's formula. That means

$$kT_{\rm equiv} = \frac{h\nu}{\exp[h\nu/kT_{\rm phys}] - 1} \tag{11}$$

The total noise contribution for the optical system is

$$T_n^{total} = T_{n1} + \frac{T_{n2}}{t_1} + \frac{T_{n3}}{t_1 t_2} + \frac{T_{n4}}{t_1 t_2 t_3} + \cdots \tag{12}$$

The total estimated noise contribution is $T_{\rm RF} = 244$ K.

The total receiver noise at 4.2 K is $T_{\rm receiver} = 1727$ K and can be divided into:

$$T_{\rm receiver} = T_{\rm RF} + L_{\rm RF}T_{\rm mixer} + L_{\rm conv}T_{\rm IF} \tag{13}$$

Using the values estimated for T_{RF}, L_{RF}, L_{conv} and T_{IF}, we estimate $T_{mixer} \approx 139$ K.

Using Tucker's theory in the 3-port approximation,[20] we calculate that the intrinsic conversion loss of the SIS junction is around 7.9 dB (DSB) at 850 GHz and the mixer noise temperature is 126 K. This is in reasonable agreement with the measured values (9.1 dB and 139 K). The embedding impedance used in the Tucker theory calculation is derived from our circuit simulation.

In summary, we have designed and fabricated Nb SIS mixers with normal metal Al tuning structures for the 1 THz band. FTS spectrum has shown the successful design of our tuning cicuit. Heterodyne mixing was performed from 822-1042 GHz and a double-sideband *corrected* receiver noise temperature of 770 K was obtained at a temperature of 2 K through this bandwidth. It may be possible to further reduce the receiver noise by optimizing the optical components. Our work demonstrates that Nb junctions can offer superior performance at terahertz frequencies when implemented with low-loss normal-metal Al tuning structures. Further advances in terahertz SIS mixers may be possible using circuits fabricated with higher-gap superconductors such as niobium nitride (NbN). However, this will require high-quality films with low RF surface resistance at terahertz frequencies.

Acknowledgements

We thank Paul Stockman and Geoff Blake for their assistance with the far-IR laser measurements, and Peter Zimmerman for providing the solid-state local oscillators. This work was supported by NASA grants NAG2-744 and NAGW-107, the NASA/JPL Center for Space Microelectronics Technology, and a NSF Presidential Young Investigator grant to J. Zmuidzinas.

REFERENCES

[1] J. Carlstrom and J. Zmuidzinas, to appear in *Review of Radio Science 1992–1995*, ed. W. Ross Stone, Oxford Science Pub. (1996).

[2] M. C. Gaidis, M. Bin, D. Miller, J. Zmuidzinas, H.G. Leduc, and J. A. Stern, to appear in Supercond. Sci. Tech. (1996).

[3] J. W. Kooi, M. S. Chan, B. Bumble, H. G. LeDuc, C. K. Walker, and T. G. Phillips, in these proceedings.

[4] G. de Lange, C. E. Honingh, J. J. Kuipers, H. H. A. Schaeffer, R. A. Panhuyzen, T. M. Klapwijk, H. Van de Stadt and M. M. W. M. de Graauw, Appl. Phys. Lett. **64**, 3039 (1994).

[5] W. C. Danchi and E. C. Sutton, J. Appl. Phys. **60**, 3967 (1986).

[6] M. J. Wengler and D. P. Woody, IEEE J. Quantum Electron. **6**, 613 (1987).

[7] D. Winkler and T. Claeson, J. Appl. Phys. **62**, 4482 (1987).

[8] M. Bin, M. C. Gaidis, J. Zmuidzinas, T. G. Phillips, and H. G. LeDuc, to appear in *Appl. Phys. Lett.* (March,1996).

[9] H. Van de Stadt, A. Baryshev, P. Dieleman, T. Klapwijk, S. Kovtonyuk, G. de Lange, I. Lapitskaya, J. Mees, R. Panhuyzen, G. Prokopenko and H. Schaeffer, Proc. Sixth Intl. Symp. Space Terahertz Tech., March 21-23, Caltech, Pasadena, CA (1995).

[10] M. C. Gaidis, M. Bin, D. Miller, J. Zmuidzinas, H.G. Leduc, and J. A. Stern, to appear in *IEEE Trans. Microwave Theory Tech.* (1996).

[11] R. L. Kautz, J. Res. Natl. Bureau Std. 84, 247 (1979).

[12] A. B. Pippard, *Advances in Electronics and Electron Physics*, vol. VI, L Marton Ed., (New York:

Academic Press, 1954), pp. 1-45.

[13] N. W. Ashcroft and N. D. Mermin, *Solid State Physics*, (Holt, Rinehart, and Winston, New York, 1976).

[14] D. C. Mattis and J. Bardeen, Phys. Rev. **111**, 412 (1958).

[15] R. Pöpel, in *Superconducting Quantum Electronics*, V. Kose, ed. (Berlin: Springer-Verlag, 1989) pp. 44-78.

[16] M. Bin, M. C. Gaidis, J. Zmuidzinas, T. G. Phillips, and H. G. LeDuc, to appear in Supercond. Sci. Tech., 1996..

[17] J. Zmuidzinas and H. G. LeDuc, *IEEE Trans. Microwave Theory Tech.* **40**, 1797 (1992).

[18] E. Hammerstad and O. Jensen, IEEE MTT-S Int. Microwave Symp. Dig., 1980, pp. 407-409.

[19] J. Zmuidzinas, H. G. LeDuc, J. A. Stern, and S. R. Cypher, *IEEE Trans. Microwave Theory Tech.* **42**, 698 (1994).

[20] J. R. Tucker and M. J. Feldman, Rev. Mod. Phys. **57**, 1055 (1985).

[21] Q. Hu, C. A. Mears, and P. L. Richards, *Int. J. IR and MM Waves*, vol. 9, no. 4, pp. 303-320, 1988..

[22] T. H. Büttgenbach, H. G. LeDuc, P. D. Maker and T. G. Phillips, *IEEE Trans. Microwave Theory Tech.*, vol. 2, no. 3, pp. 165-175, 1992..

[23] D. P. Woody, R. E. Miller and M. J. Wengler, *IEEE Trans. Microwave Theory Tech.* **33**, 90 (1985).

[24] N. Dubash, M. J. Wengler, and J. Zmuidzinas, *IEEE Trans. Appl. Superconductivity* **5**, 3308 (1995).